JOURNAL OF APPLIED ELECTROCHEMISTRY 21 (1991) 14–20

# Electrochemical waste water treatment using high overvoltage anodes. Part I: Physical and electrochemical properties of $SnO_2$ anodes

R. KÖTZ*, S. STUCKI*, B. CARCER

*Asea Brown Boveri, Corporate Research CRB, CH-5405 Baden, Switzerland*

Received 13 December 1989; revised 10 April 1990

The electrochemical performance of $SnO_2$ as an anode material with high oxygen gas-evolution overpotential was investigated in view of its application for electrochemical oxidation of bio-refractory organics in waste waters. The influence of the doping agent (Sb, F, Cl) and doping level on the oxygen-evolution reaction was studied in terms of Tafel slope, oxygen-overpotential and exchange current densities for the $Ce^{3+} \rightarrow Ce^{4+}$ reaction. Tafel slopes of about 300 mV decade$^{-1}$ were found and the oxygen evolution overpotential was 600 mV higher than that of platinum. While the doping level had no significant influence on Tafel slopes and oxygen overpotentials the stability of the $SnO_2$ electrode increased with charge carrier density. The oxidation of phenol was investigated as a test for the oxidizing power of the new anode material when compared to Pt or $PbO_2$. The rate of phenol removal was much higher for $SnO_2$ than for $PbO_2$ or Pt.

## 1. Introduction

The anodic evolution of oxygen in aqueous electrolytes has been studied for many years in search of a stable anode material with *low* oxygen evolution overvoltage. Such anode materials allow considerable voltage savings in technical electrolysis processes and make them more cost efficient. The $RuO_2$-based DSA® electrode for chlorine evolution and the mixed $RuO_2/IrO_2$ anode catalyst for oxygen evolution in the ABB-Membrel® electrolyzers are two examples.

There are, however, other processes, like the anodic oxidation of organic molecules [1–11] or ozone generation [12, 13], where a *high* oxygen evolution overvoltage is desirable. For such processes anodic oxygen evolution in aqueous electrolytes represents an unwanted leakage current, reducing the overall current efficiency and the available oxidation potential. Standard electrode materials which are used as anodes with high oxygen evolution potential are platinized titanium (Pt/Ti), graphite or lead dioxide. While the former material (Pt/Ti) with a moderate overpotential has the disadvantage of being expensive, the latter are not stable under technical electrolysis conditions.

We have investigated tin dioxide ($SnO_2$) as an alternative electrode material with high oxygen evolution overpotential for the anodic oxidation of bio-refractory organics i.e. organic pollutants which are not decomposed by microorganisms under normal conditions. Pure $SnO_2$ is an n-type semiconductor with a direct band gap of roughly 3.5 eV and can be used as an electrode material with reasonable conductivity only at high temperatures. Doped $SnO_2$ has been used as a transparent electrode material in photoelectrochemistry. The electrochemical properties of polycrystalline as well as single crystalline, $SnO_2$ were investigated by several researchers. A comprehensive review was prepared by Manthakma and Armstrong [14]. The physical properties and preparation procedures were reviewed by Jarzebski and Marton [15–18]. The combination of (i) high chemical and electrochemical stability as a consequence of the rather large band gap, (ii) high electrical conductivity of doped $SnO_2$ and (iii) the high oxygen evolution overpotential makes $SnO_2$ an attractive electrode material for the anodic oxidation of organics in aqueous solutions.

## 2. Experimental details

### 2.1. *Electrode preparation*

$SnO_2$ film electrodes were prepared by the standard spray hydrolysis method [15, 18]. An alcoholic solution of $SnCl_4 \times H_2O$ was sprayed onto the heated titanium substrate at temperatues of around 500° C using commercially available spray guns (Badger Air-Brush Co). Nitrogen served as the transporting gas. Doping with antimony or fluorine was achieved by addition of $SbCl_3$ or $NH_4F$ to the spray solution. The titanium substrates were previously etched in 10% oxalic acid. The best composition of the spray solution was found to be 10 g $SnCl_4 \times 5H_2O$, 0.1 g $SbCl_3$ in

* Present address: Paul Scherrer Institute, CH-5232 Villigen PSI, Switzerland.



0021-891X/90 $03.00 + .12 

100 ml of ethanol. Results reported below refer to this composition.

For resistivity measurements films were sprayed onto quartz substrates, and their thickness was determined by means of a profilometer. Film thicknesses were typically 1–4 $\mu$m. Some experiments were performed on bulk ceramic $SnO_2$ electrodes prepared after a proprietary method.

### 2.2. *Electrode analysis*

Charge carrier densities were determined by means of Mott-Schottky plots using a Solatron Frequency Response Analyser (Solatron 1170) and a Solatron Electrochemical Interface (Solatron 1186). The $1/C^2$ curves were obtained at 1000 Hz in 0.1 N $H_2SO_4$ with 20 mV modulation amplitude. Electrochemical measurements were performed using the standard three electrode arrangement with a platinum wire in a separate compartment as counter electrode and a saturated calomel electrode as a reference electrode. Electrolytes were prepared from ultra pure reagents and triply distilled water.

Rotating disc electrode measurements were performed on a Jaissle SRE 74 rotating ring disc system for determination of the Tafel curves for the $Ce^{3+} \rightarrow Ce^{4+}$ oxidation reaction. The disc had 1 $cm^2$ surface area. The exchangable $SnO_2$ disc electrode was prepared by spraying the $SnCl_4$ solution onto a titanium cylinder.

XPS investigations were performed on a Kratos ES300 electron spectrometer equipped with an electrochemical preparation chamber [19] using Mg $K\alpha$ radiation.

Determination of the total organic carbon (TOC) in the model electrolytes was performed using Shimazu TOC500. The concentration of Phenol (and other organic model compounds) was determined by means of UV-VIS derivative absorption spectroscopy (Shimazu UV-160). Before optical concentration determination the samples were adjusted to pH 1.

### 2.3. *Degradation tests*

Experiments were run on two different scales: tests on electrodes up to 10 $cm^2$ of electrode area were performed in a simple stirred beaker cell with a platinized titanium counter electrode (no reference electrode) and an electrolyte volume of 150 ml. For tests in alkaline electrolyte pure titanium cathodes were used.

A bench scale general purpose reactor from ElectroCell AB (SU Electro MP-cell, 0.01 $m^2$) was used for the evaluation of the relevant process engineering parameters, which will be described in part II.

## 3. Results and discussion

### 3.1. *Preparation and physical properties*

Several different preparation methods for $SnO_2$ films have been described in the literature [14–18]. The spray pyrolysis method was chosen for our studies, because this method is relatively simple and inexpensive, reproducible, and appears to be suitable for technical mass production. The influence of the two main parameters for $SnO_2$ film preparation using this method, i.e. substrate temperature and doping level were studied systematically. Figures 1 and 2 show the specific film resistivity as a function of the substrate temperature and the doping level for antimony and fluorine doping. Doping was achieved by addition of different amounts of $SbCl_3$ or $NH_4F$ to the spraying solution. The three curves in Fig. 1 exhibit a minimum in resistivity at a temperature between 400 and 500° C. The lowest specific resistivity of about $7 \times 10^{-4}$ Ωcm is obtained with fluorine at a concentration of about 30 mol % in the spray solution. For antimony the lowest resistivity is $1 \times 10^{-3}$ Ωcm at 5 mol % of antimony in the solution. Without any dopant, i.e. only residual chlorine doping, a minimum resistivity of $2 \times 10^{-2}$ Ωcm was achieved.

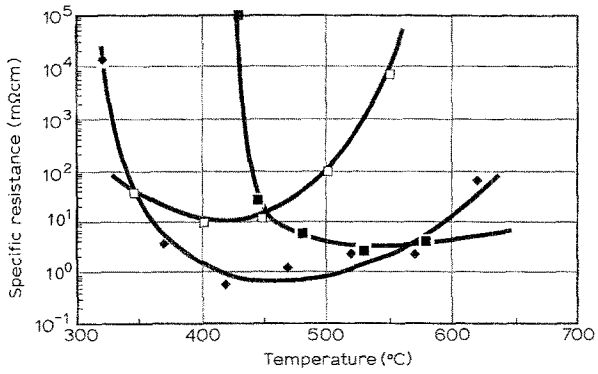


Fig. 1. Specific resistivity of $SnO_2$ films prepared by the spray hydrolysis method on quartz substrates as a function of substrate temperature. Dopant: (□) chlorine, (◆) fluorine and (■) antimony.

In the case of antimony doping the actual Sb content of the film was determined by means of XPS. The $Sb3d_{3/2}$ level exhibited a binding energy of 589.8 eV, indicating antimony in the valence state V. A linear correlation was found for the mole % of antimony in the spray solution and in the film with a slope of close to one. These findings are in good agreement with literature [18]. XPS analysis for the determination of fluorine-concentrations in the $SnO_2$ films

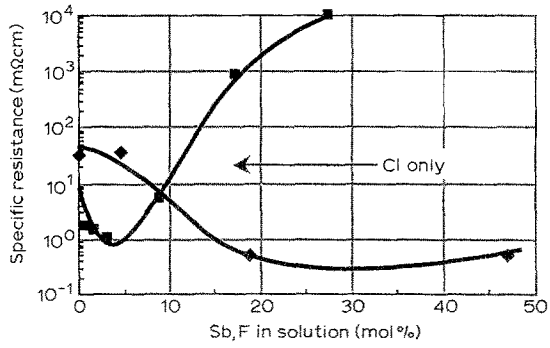


Fig. 2. Specific resistivity of antimony (■) and fluorine (◆) doped $SnO_2$ films prepared by the spray hydrolysis method on quartz substrates as a function of mol % of the doping agent in the spray solution.

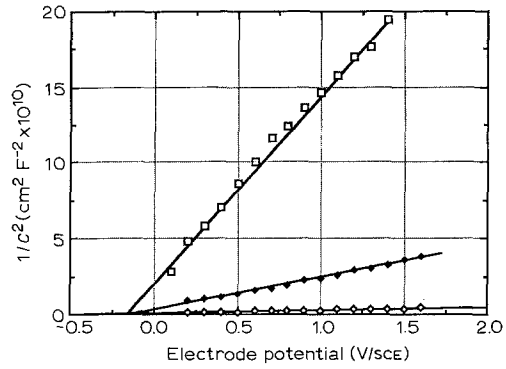


Fig. 3. Mott-Schottky plots for $SnO_2$ electrodes in 1 N $H_2SO_4$ for three different antimony doping levels: (□) 0%, (◆) 0.5% and (◇) 4.0% Sb. For 0%, doping is achieved by residual chlorine.

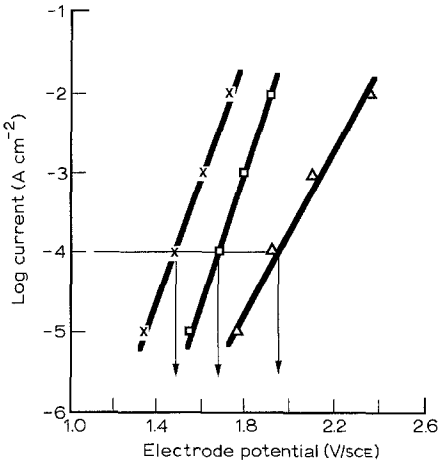


Fig. 4. Comparison of anodic Tafel lines during oxygen evolution in 1 N $H_2SO_4$ on (×) Pt, (□) $PbO_2$ and (△) Sb (4 mol %) doped $SnO_2$.

was not successful. Inspite of the high $NH_3F$ concentrations in the spray solution, fluorine doping levels are below the detection limit of the XPS system.

Introduction of a dopant to a semiconducting material leads to free charge carriers which, in combination with their mobility, determine the electrical conductivity (resistivity) of the material. The charge carrier density was determined from $1/C^2$ plots following the Mott-Schottky procedure. Mott-Schottky plots for different antimony concentrations are shown in Fig. 3. Good linear correlations are obtained for a potential range of 1.5 V which corresponds to roughly half of the band gap. The flat band potential was determined to be $-150\,mV_{sce}$. The resulting charge carrier density as a function of Sb mol % in the film reveals a maximum of about $5 \times 10^{21}\ cm^{-3}$ at about 7% of antimony. For the calculation of the charge carrier density a roughness factor of one was assumed and the dielectric constant was set to 10 with an effective mass of the electron of 0.5. The discrepancy between antimony concentration necessary for achieving minimum resistivity (Fig. 2) and maximum charge carrier density is a consequence of decreasing mobility with increasing carrier densities.

### 3.2. *Electrochemical properties of $SnO_2$*

*3.2.1. Oxygen evolution.* The cyclic voltammogram of $SnO_2$ electrodes is nearly featureless in the steady state after several cycles. At the anodic end oxygen evolution occurs, while at the cathodic end $SnO_2$ reduction and hydrogen evolution lead to significant cathodic currents [20]. At low scan rates additional features may arise from ion adsorption as was demonstrated by Laitinen *et al.* [21]. A comparison of Tafel lines for anodic oxygen evolution at standard electrode materials like platinized titanium or $PbO_2$ and the new $SnO_2$ electrode is given in Fig. 4 in 0.1 N $H_2SO_4$.

At a reference current density of $0.1\,mA\,cm^{-2}$ the oxygen evolution potential increases from 1.5 to $1.65\,V_{sce}$ and to $1.95\,V_{sce}$ for Pt, $PbO_2$ and $SnO_2$, respectively. At higher current densities the increase in oxygen overpotential is even more marked for the $SnO_2$ anode because the Tafel slope is $240\,mV\,decade^{-1}$ compared to roughly $120\,mV\,decade^{-1}$ for Pt and $PbO_2$. At $10\,mA\,cm^{-2}$, which is a reasonable current density for technical applications, the oxygen evolution potential of $SnO_2$ is by 650 mV higher than that of the platinum anode under the same conditions.

The influence of the dopant concentration of $SnO_2$ electrodes on the oxygen evolution overpotential and on the Tafel slope in 0.1 N $H_2SO_4$ is given in Fig. 5. Both parameters appear to be unaffected by the charge carrier density of the semiconducting material. The Tafel slope was determined to be 290 ± 50 mV $decade^{-1}$ and the oxygen evolution potential for a current density of 0.1 mA was found to be 2.2 ± 0.1 V. Thus the observed characteristic values for $SnO_2$ are not significantly altered by the dopant. Obviously, electronic charge transfer is not the rate determining step for oxygen evolution, because the observed reaction rate does not depend on the width of the potential barrier in case of electron tunneling or on the number of available electronic states. In order to gain more insight into electron transfer at highly doped $SnO_2$ electrodes the outer sphere electron transfer reaction of the cerium redox couple was investigated.

*3.2.2. Cerium oxidation.* The anodic one electron charge transfer reaction $Ce^{3+} \rightarrow Ce^{4+} + e^-$ was investigated. The $Ce^{3+}/Ce^{4+}$ couple was chosen because of its redox potential of $1.5\,V_{rhe}$ is above the reversible

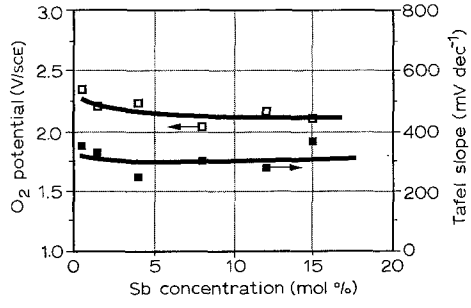


Fig. 5. Tafel slopes and oxygen evolution overpotentials at 0.1 mA $cm^{-2}$ for anodic oxygen evolution on $SnO_2$ electrodes doped with antimony in 0.1 N $H_2SO_4$.

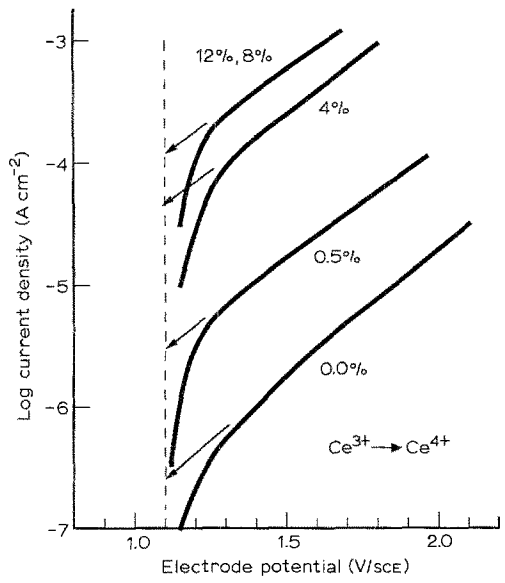


Fig. 6. Current-potential curves for the cerium oxidation reaction on $SnO_2$ as a function of electrode potential in 1 N $H_2SO_4$ and $7 \times 10^{-3}$ mol $Ce^{3+}$. Sb doping level is given at each curve (in %).

water splitting potential. The results for various antimony dopings are plotted in Fig. 6 and indicate constant Tafel slope for the Ce oxidation reaction, but increasing exchange current density with increasing charge carrier densities. The rather high Tafel slope of about 450 mV decade$^{-1}$ is typical for semiconductor behaviour [22]. Identical results were obtained by means of a rotating $SnO_2$ disc electrode experiment where the true kinetic currents were determined by extrapolation of the measured currents to infinite rotation speed.

For doped $SnO_2$, direct tunneling of electrons into the conduction band may be considered as a possible mechanism for charge transfer. The relatively high concentration of charge carriers results in a rather narrow charge barrier, the width of which decreases with increasing carrier density. Therefore the tunneling probability and the reaction rates should increase with the doping level. From Fig. 6 such a relation can be deduced. The cerium oxidation currents increase by more than two orders of magnitude when the charge carrier density is increased from $1 \times 10^{20}$ to $5 \times 10^{21}$ cm$^{-3}$. This is qualitatively in agreement with tunneling probabilities, which were calculated according to the equation given in [23, 24] for a redox potential of 1.1 $V_{sce}$ and a flat band potential of $-0.15$ $V_{sce}$. The dielectric constant of $SnO_2$ was assumed to be 10 and the electron effective mass was 0.5. For the oxygen evolution reaction, however, the anodic reaction rate does not depend on the charge carrier density as is evident from Fig. 4. Obviously direct tunneling may be rate determining for the outer sphere $Ce^{3+}$ oxidation-reaction, but not for the inner sphere reaction of anodic water oxidation, where adsorption effects have to be considered.

*3.2.3. Stability and substrate effects.* In view of a technical application of $SnO_2$ anode material for anodic oxidation of bio-refractory waste water, stability of the electrode material is important. While the short term performance of the $SnO_2$ films turned out to be independent of the substrate, the long term stability of the $SnO_2$ film electrodes depends significantly on the substrate used. Pure titanium substrates, operated at constant current density, passivate as indicated by a significant increase in cell voltage. Probably the $SnO_2$ film with a typical thickness of 2–5 $\mu$m does not sufficiently protect the titanium underneath.

The operating time of electrodes could be influenced by a thermal annealing at elevated temperatures in air prior to use. The best annealing process turned out to be 1 h at 600° C in air. In addition, the life-time of the $SnO_2$/Ti electrodes increased with increasing pH of the electrolyte. Investigation of $SnO_2$ film electrodes on titanium before and after prolonged anodic oxygen evolution by means of EDX and XPS did not reveal any significant changes of the film thickness (Sn/Ti ratio in EDX) or the antimony content of the surface layer (XPS, Fig. 8). Passivation was also observed on tantalum, nickel, tungsten and molybdenum substrates.

In order to determine the stability of $SnO_2$ without any possible substrate effects we have performed additional long term tests on bulk ceramic antimony doped $SnO_2$ electrodes, prepared by sintering using a proprietory method. Electrodes were tested at 20 mA cm$^{-2}$ current density until the electrode potential had increased from initially 2.3 to 3.0 $V_{sce}$.

From Fig. 7 it becomes clear that the rate of potential increase (inverse lifetime) of the antimony doped $SnO_2$ electrodes is strongly related to the charge carrier density. The higher the doping level, the lower the rate of potential increase. This is in accord with a qualitative model for electrode passivation. The transition from non-passivating behaviour to passivation depends on the electronic and ionic conductivity of the surface layer formed on the electrode. If the electronic conductivity is below a certain threshold value, the electric field in the layer increases to the point where ions become mobile. As a consequence the electrochemical interface shifts away from the surface into the bulk of the electrode, increasing the surface layer thickness and eventually leading to passivation. Figure 8 shows the XPS spectra for Sn3d, Sb3d and O1s of a $SnO_2$ film electrode before and after anodic

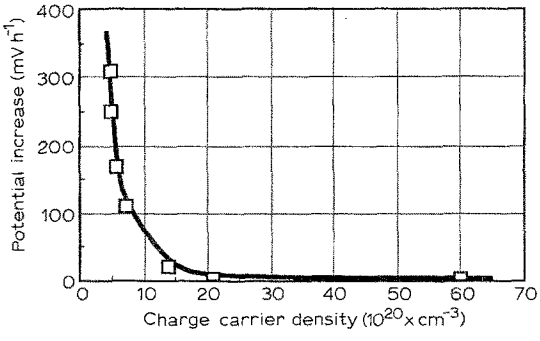


Fig. 7. Rate of potential increase during anodic oxygen evolution on ceramic $SnO_2$ doped with antimony in 0.1 N NaOH as a function of the charge carrier density. Current density: 20 mA cm$^{-2}$.

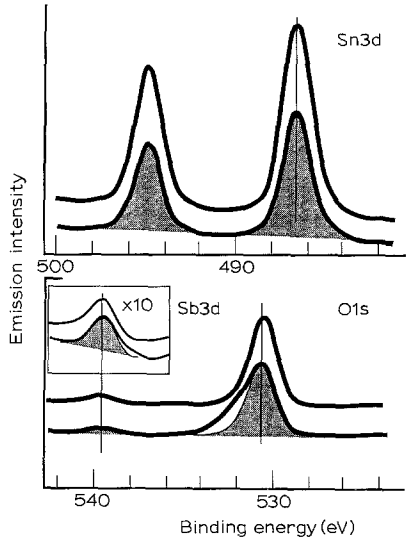


Fig. 8. XPS spectra of a $SnO_2$ film electrode on titanium before (upper) and after (lower curves) oxygen evolution at 2.5 V for 30 min in 1 N $H_2SO_4$. Shaded areas are projections of the upper spectra onto the lower spectra for better comparison.

oxygen evolution. As stated, above, no changes in Sb/Sn ratio or for the oxidation state of Sn can be detected. The O1s level, however, is slightly broadened towards higher binding energies indicating OH formation. The passivating surface layer is probably formed by hydration of the $SnO_2$. The results show that passivating phenomena occur on both, the $SnO_2$ surface and the substrate-film interface.

*3.2.4. Phenol oxidation.* So far, we have dealt with the oxygen evolution, which is the side reaction competing with oxidation of organics in the electrolyte. For the investigation of anodic oxidation of organic wastes we have chosen phenol as test molecule (tests with benzoic acid, which is more difficult to oxidize, and other model compounds are described in part II) because the oxidation of phenol has been investigated by several authors with respect to oxidation by ozone [25–28] and electrochemically [4, 7–10]. Figure 9 shows the disappearance of the substance and of the total organic carbon (TOC) in a galvanostatic run using the $SnO_2$ anode in 0.5 N $Na_2SO_4$ (pH 12) as a function of the charge consumed. While phenol disappears after 1 Ah, the complete removal of TOC takes about 8 Ah. The fact that TOC can be eliminated almost completely, indicates that phenol is mainly oxidized to $CO_2$ (i.e. carbonate).

A comparison of typical electrode materials like platinized titanium and lead dioxide with the performance of the new $SnO_2$ electrode is given in Fig. 10 for TOC removal during phenol oxidation. The $SnO_2$ electrode exhibits higher efficiency for TOC elimination than Pt or even $PbO_2$. For the total elimination of TOC at $SnO_2$ 8 Ah are needed, whilst Pt as well as $PbO_2$ remove TOC rather ineffectively. The low efficiency of Pt and $PbO_2$ is due to the relatively large leakage current for oxygen evolution. In additon, it has been demonstrated for platinum anodes, that the oxidation reaction stops with products like maleic acid or oxalic acid [11]. Assuming a cell voltage of 4 V, which is realistic for a technical application, elimination of 1 kg of phenol (1 $m^3$ with 1000 p.p.m.) consumes 20 kWh, for the elimination of 1 kg of TOC 110 kWh are needed.

The results with phenol show that the use of a $SnO_2$ anode increases the current efficiencies for TOC removal in waste water significantly (see Fig. 10 for phenol; the performance of $SnO_2$ for other organic molecules is presented in part II) and will potentially make this electrochemical process technically interesting. Aspects of the technical application and process design is discussed in part II. In the following the superiority of $SnO_2$ over Pt and $PbO_2$ with respect to anodic oxidation of organics is discussed.

*3.2.5. Mechanistic aspects.* The band gap of $SnO_2$ thin films prepared in our laboratory is about 4.1 eV as determined by means of optical absorption measurements. From Mott-Schottky plots the flat band potential in pH 1 electrolyte can be estimated to be at $-200\,mV_{sce}$. Thus the band bending during anodic oxidation at 10 mA $cm^{-2}$ is about 2.5 V, which is roughly half of the band gap. As a consequence of the low lying valence band and of the fact that $SnO_2$ is an n-type semiconductor, valence band reactions can be ruled out for the anodic oxidation of water or organic constituents.

In order to gain more insight into the actual composition of the electrode surface XPS investigations

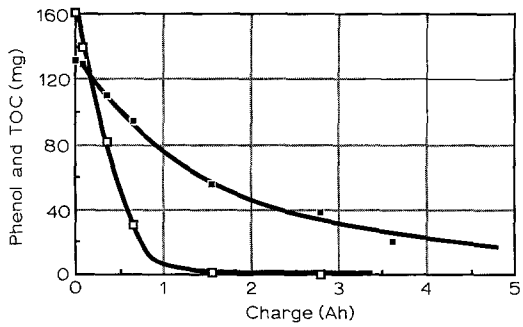


Fig. 9. Removal of 1000 p.p.m. phenol (□) and respective total organic carbon TOC (■) by anodic oxidation using a $SnO_2$ anode at 30 mA $cm^{-2}$ in pH 12 electrolyte as a function of charge consumed.

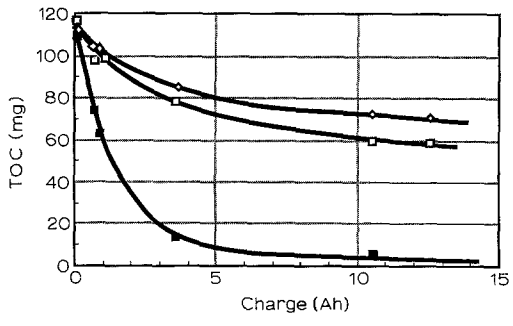


Fig. 10. Removal of total organic carbon (TOC) originating from 1000 p.p.m. phenol in the electrolyte as a function of consumed charge for different electrode materials for: (■) $SnO_2$, (□) $PbO_2$ and (◇) Pt. Current density: 30 mA $cm^{-2}$.

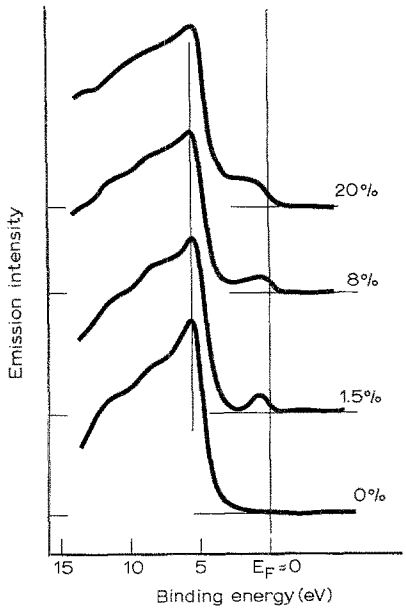


Fig. 11. XPS valence band spectra of $SnO_2$ electrodes (on quartz) as prepared for various concentrations of antimony (in %) in spray solution. XPS (Mg Kα) energy: 1253.6 eV.

were performed on $SnO_2$ electrodes, doped with various amounts of antimony. The results are given in Fig. 11 and show a considerable density of states in the band gap when antimony is introduced into the film. Without antimony doping no electronic states are detected within the band gap. For antimony concentrations $\geqslant 1.5\%$ electronic states are observed about 0.5 eV below the Fermi level, indicating conduction band filling, giving rise to a semiconductor-to-metal transition. With increased doping the band gap is completely filled. Similar observations were made by Egdell *et al.* [29, 30] for polycrystalline $SnO_2$. These authors found a pronounced enrichment of antimony close to the surface of doped $SnO_2$. The surface antimony, however does not contribute to the free carrier concentration. Filling of the band gap at higher antimony level may originate from a surface state, associated with segregated antimony ions, located at the top of the valence band.

From the XPS measurements it is clear that holes are available at the surface of the antimony doped $SnO_2$ anode and oxidation of organics may proceed via a hole mechanism. This assumption may also explain the different oxidation reaction paths and efficiencies observed for $SnO_2$ and Pt (see Fig. 10), because an increased residence time (lower hole mobility) of the adsorbate on the substrate is to be expected for such a mechanism. Increased residence times for the organic adsorbate as well as for $H_2O$ may result in different oxidation mechanisms compared to standard electrodes. While organics may be partly cracked down to $CO_2$, in the case of water highly reactive intermediates like OH* or ozone may be created. In fact it has been demonstrated by Foller and Tobias [12] that ozone evolution occurs on $SnO_2$ at high current densities. These results were reproduced in our laboratory and it was demonstrated that the current efficiency for ozone generation is even higher on $SnO_2$ than on $PbO_2$. $SnO_2$ electrodes are, however, not stable under $O_3$ generating conditions and it is not clear whether the ozone reaction also proceeds at the low current densities involved with anodic oxidation of organics.

The difference in reaction mechanisms is nicely evidenced in the case of phenol oxidation. The electrochemical oxidation of phenol has been investigated by various authors [4, 7, 9]. Using traditional electrode materials the oxidation has been found to produce benzoquinone as the first intermediate. If an undivided cell is used benzoquinone is partially reduced to hydroquinone, establishing a reversible redox couple which entails parasitic current consumption. Further oxidation of benzoquinone leads to break up of the aromatic ring and yields maleic acid as a relatively stable intermediate, which is then converted to $CO_2$ in a reaction with much reduced current efficiency. The same reaction scheme has been found to be followed by platinum anodes as well as by lead dioxide electrodes. The oxidation scheme, including the appearance of the quinone/hydroquinone redox couple, was confirmed in our experiments using platinized titanium anodes (Fig. 12).

The $SnO_2$ electrode shows a marked difference to the platinized titanium: no quinone intermediates are formed, which means that either the quinones are much more rapidly oxidized by $SnO_2$ than by platinum or that ring opening occurs as the first step with phenol. The rate of phenol oxidation and the rate of TOC removal are considerably higher for $SnO_2$ than for platinum electrodes under otherwise identical experimental conditions.

## 4. Conclusions

The oxidation efficiency of the high overvoltage anode material $SnO_2$ with antimony doping using phenol as a test molecule, has been shown to be superior to the state-of-the-art electrode materials $PbO_2$ and Pt. The achievable oxidation potential is 650 mV higher than that of platinum. While the stability of the electrode and the outer sphere $Ce^{3+}$ oxidation reaction depends very much on the charge carrier density, the anodic oxygen evolution process appears to be unaffected.

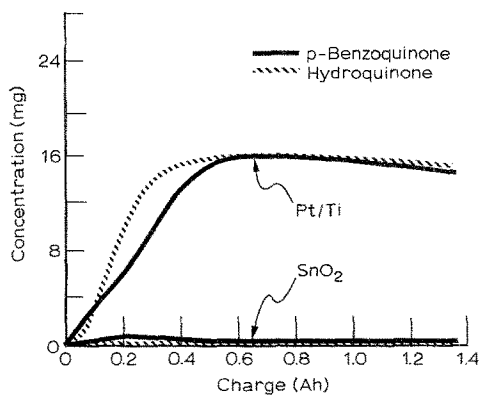


Fig. 12. Build-up of p-benzoquinone (——) and hydroquinone (– – –) during degradation of (40 mg) phenol at Pt and $SnO_2$ anodes in 1 N $H_2SO_4$. Current density: 5 mA cm$^{-2}$.

The mechanism of the oxidation reactions involved is not known. A hole reaction mechanism for the charge transfer at the $SnO_2$ surface is suggested on the basis of XPS results. Doping of $SnO_2$ with antimony creates a considerable density of states in the band gap of the semiconductor.

## References


[1] S. D. Ross, M. Finkelstein and E. J. Rudd, 'Anodic Oxidation' Academic Press, New York (1975).
[2] M. Josowicz, in 'Anodische Oxidation in der Wasser- und Lufthygiene' (edited by A. Reis), G-I-T Verlag/ E. Giebeler, Darmstadt (1981) p. 133.
[3] E. Plattner and C. Comninellis, in 'Process Technologies for Water Treatment' (edited by S. Stucki) Plenum, New York (1988) p. 205.
[4] V. Smith de Surce and A. P. Watkinson, *Canadian J. Chem. Eng* **59** (1981) 52.
[5] J. A. Harrison and J. M. Mayne, *Electrochimica Acta* **28** (1983) 1223.
[6] D. W. Kirk, H. Sharifian and F. R. Foulkes, *J. Applied Electrochem.* **15** (1985) 285.
[7] D. T. Chin and C. Y. Cheng, *J. Electrochem. Soc.* **132** (1985) 2605.
[8] D. Wabner, C. Grambow and A. Ritter, *Vom Wasser* **64** (1985) 269.
[9] H. Sharifian and D. W. Kirk, *J. Electrochem. Soc.* **133** (1986) 921.
[10] I. F. McConvey, K. Scott, J. M. Henderson and A. N. Haines, *Chem. Eng. Process.* **22** (1987) 231.
[11] C. Comninellis and E. Plattner, *Chimia* **42** (1988) 250.
[12] P. C. Foller and C. W. Tobias, *J. Electrochem. Soc.* **129** (1982) 506.
[13] R. Kötz and S. Stucki, *J. Electroanal. Chem.* **228** (1987) 407.
[14] A. Nanthakumar and N. R. Armstrong, Tin Oxide ($SnO_2$), Indium Oxide ($In_2O_3$) and Tungsten Oxide ($WO_3$), in 'Semiconductor Electrodes' (edited by H. O. Finklea), Elsevier, Amsterdam (1988) p. 203–41.
[15] Z. M. Jarzebski and J. P. Marton, *J. Electrochem. Soc.* **123** (1976) 199C.
[16] *Idem, ibid.* **123** (1976) 299C.
[17] *Idem, ibid.* **123** (1976) 333C.
[18] K. L. Chopra, S. Major and D. K. Pandya, *Thin Solid Films* **102** (1983) 1.
[19] H. Neff, F. Foditsch and R. Kötz, *J. Electron Spectr. Rel. Phen.* **33** (1984) 171.
[20] H. Kim and H. A. Laitinen, *J. Electrochem. Soc.* **122** (1975) 53.
[21] H. A. Laitinen, C. A. Vincent and T. M. Bednarski, *ibid.* **115** (1968) 1024.
[22] J. W. Schultze and L. Elfenthal, *J. Electroanal. Chem.* **204** (1986) 153.
[23] D. Elliott, D. L. Zellmer and H. A. Laitinen, *J. Electrochem. Soc.* **117** (1970) 1343.
[24] B. Pettinger, H. R. Schöppel and H. Gerischer, *Ber. d. Bunsen Gesellschaft* **78** (1974) 450.
[25] S. D. Razumovskii and G. E. Zaikow, 'Ozone and its Reactions with Organic Compounds', Elsevier, Amsterdam (1984) chapter 7, p. 272.
[26] M. D. Gurol and P. C. Singer, *Water Res.* **17** (1983) 1163.
[27] *Idem, ibid.* **17** (1983) 1173.
[28] J. Hoigne and H. Bader, *ibid.* **17** (1983) 185.
[29] P. A. Cox, R. G. Egdell, C. Harding, W. R. Patterson and P. J. Taverner, *Surf. Sci.* **123** (1982) 179.
[30] R. G. Egdell, W. R. Flavell and P. Taverner, *J. Solid State Chem.* **51** (1984) 345.